Neutralizer Hollow Cathode Simulations and Validation with Experiments

Ioannis G. Mikellides,[1] Dan M. Goebel,[2] John S. Snyder,[1] Ira Katz,[3]
Jet Propulsion Laboratory, California Institute of Technology, Pasadena, CA, 91109

and

Daniel A. Herman[4]

ASRC Aerospace Corporation, Cleveland, OH, 44135

The fidelity of electric propulsion physics-based models depends largely on the validity of their predictions over a range of operating conditions and geometries. In general, increased complexity of the physics requires more extensive comparisons with laboratory data to identify the region(s) that lie outside the validity of the model assumptions and to quantify the uncertainties within its range of application. This paper presents numerical simulations of neutralizer hollow cathodes at various operating conditions and orifice sizes. The simulations were performed using a two-dimensional axisymmetric model that solves numerically a relatively extensive system of conservation laws for the partially-ionized gas in these devices. The results for the plasma are compared directly with Langmuir probe measurements. The computed keeper voltages are also compared with the observed values. Wherever model inputs and/or specific physics of the cathode discharge are uncertain, additional sensitivity calculations have been performed to quantify the uncertainties.

Nomenclature

C_s = ion acoustic speed, m/s
I_K = keeper current, A
f = wave frequency, Hz
$\mathbf{j}_e$ = electron current density, A/m^2
$j_{e,th}$ = electron thermal current density, A/m^2
$\mathbf{j}_i$ = ion current density, A/m^2
k = ion acoustic wave number, m^{-1}
k_B = Boltzmann's constant, J/K
Kn = Knudsen number
m_i = mass of xenon ion, kg
m_e = mass of electron, kg
$\hat{\mathbf{n}}$ = normal unit vector
n_e = electron number density, particles/m^3
q_e = charge, 1.602×10^{-19} C
P = chamber background pressure, Torr
S_K = keeper current-collection area, m^2
T_e = electron temperature, K
u_e = electron drift speed, m/s
$u_{T,e}$ = electron thermal speed $(2k_BT_e/m_e)^{½}$, m/s
u_i = ion drift velocity, m/s
V_K = keeper voltage, V

Greek Symbols

λ_{mfp} = mean free path for (classical) collisions, m
ν_α = effective collision frequency, s^{-1}
ν_{ei} = electron-ion collision frequency, s^{-1}
ν_{en} = electron-neutral collision frequency, s^{-1}
$\phi_{p,s}$ = plasma(p) or sheath (s) potential, V
ω_{pe} = electron plasma frequency, rad/s

[1] Member Technical Staff, Electric Propulsion Group, 4800 Oak Grove Drive, Pasadena, CA, 91109, Mail Stop 125-109, Senior Member AIAA.
[2] Section Staff, Thermal and Propulsion Engineering Section, 4800 Oak Grove Drive, Pasadena, CA, 91109, Mail Stop 125-109, Senior Member AIAA.
[3] Group Supervisor, Electric Propulsion Group, 4800 Oak Grove Drive, Pasadena, CA, 91109, Mail Stop 125-109, Senior Member AIAA.
[4] Aerospace Engineer, Propulsion and Propellants Branch, 21000 Brookpark Road, Cleveland, OH, 44135, Mail Stop 16-1, Member AIAA.

I. Introduction

THE Orificed Cathode (OrCa2D) computer code is a two-dimensional (2-D) axisymmetric model of the plasma and neutral gas in electric propulsion (EP) hollow cathodes, and has been developed at JPL to support life assessment and EP life qualification activities for NASA's science missions. The ultimate goal of the life modeling effort is to lower the cost and risk associated with the employment of Solar Electric Propulsion on Discovery, New Frontiers and Flagship missions. The 2-D axisymmetric model simulates the partially-ionized gas that is generated by these devices, both inside the cathode channel (insert region) and outside the channel, around the orifice plate and the keeper region. It uses finite volume differencing to solve numerically the multi-species conservation equations for electrons, singly-charged xenon ions and xenon atoms, using a strongly-implicit, time-split approach.

OrCa2D was applied in the past to simulate a variety of discharge hollow cathode (DHC) geometries and operating conditions, and the results have compared well with experimental measurements both inside the device and in the near plume.[1,2] In ring-cusp ion thrusters the DHC typically operates at higher flow rate and total current than the neutralizer hollow cathode (NHC). Moreover, in these engines, the magnetic field supplied by the ring magnets plays no significant role on the evolution of the plasma in the NHC plume. Finally, the current collected by the keeper electrode in a NHC is usually a substantial portion of the total current (beam + keeper current) and the cathode-plate orifice is smaller in diameter compared to a DHC for a given ion engine. These differences combined lead to distinctively different plasma properties in NHCs compared to DHCs that can have important implications on life-limiting mechanisms, such as plume mode, cathode-plate orifice erosion and keeper erosion.

This computational effort was motivated in part by NHC performance results observed during the NEXT Life Demonstration Test (LDT). NEXT (NASA's Evolutionary Xenon Thruster) is an advanced ion propulsion system developed by a team led by the NASA Glenn Research Center (GRC) consisting of a 7-kW, 36-cm ion thruster, power processing unit, propellant management system, and gimbal.[3] LDT performance trends over the first 10 khr of operation include a measureable drop in neutralizer keeper voltage that, while not particularly concerning, was not completely understood. Of greater concern was the loss of plume mode flow margin, the difference between the operating flow rate and the flow rate at the transition from "spot mode" to "plume mode," which showed significant changes including negative flow margin at some operating conditions based on the NEXT Projections throttle table.[4] The modeling work discussed herein is aimed at understanding these changes and identifying corrective actions.

Before offering critical insight on engine test observations using the model results, the validity and uncertainties of the model must first be established. The work presented in this paper extends the validation of OrCa2D by comparing numerical simulation results for the plasma and for the predicted circuit parameters with laboratory measurements. To establish the model's fidelity we compare results for three different NHC orifice sizes at four different operating points with the objective of covering a wide range of plasma conditions. For most cases presented in this paper the discharge in the laboratory appears quiescent with little to no fluctuations in the circuit parameters; operation of the cathode under these conditions is known as "spot mode."

II. Neutralizer Hollow Cathode Simulations and Comparisons with Laboratory Data

A. The Computational Model

1) General description

The features and conservation equations of the two-dimensional computational model OrCa2D used for the NHC plasma simulations has been described in detail in previous articles[5,1] and will only be described briefly here. The model solves the conservation laws for three species present in the partially-ionized gas: electrons, xenon ions and xenon neutrals. It is assumed that only singly-charged ions are present and that the ionized species satisfy quasi-neutrality. The equations of continuity and momentum for ions, and the momentum equation for the electrons, are solved directly to yield the plasma particle density, ion and electron current densities. The combination of the electron

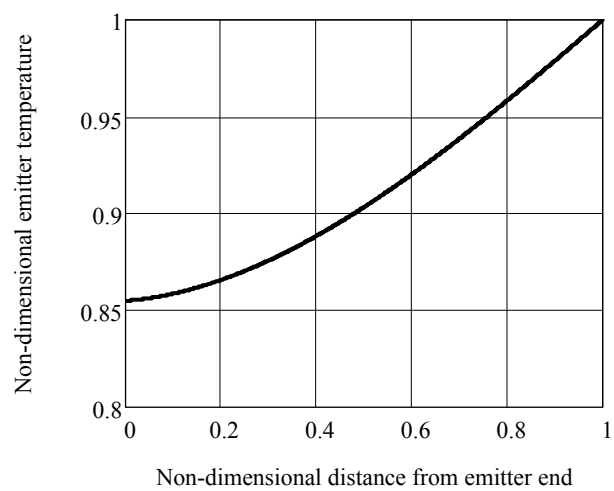

Fig. 1 The emitter temperature profile used in the NHC numerical simulations is based on measurements performed by Polk, et al.[4] The peak emitter temperature $T_{w,max}$ is an input value to the model.

and ion continuity equations yields the current conservation law, which is solved implicitly in OrCa2D to obtain the plasma potential. All relevant elastic and inelastic collision frequencies are included in the transport terms. The electron temperature is obtained from the electron energy transport equation, which includes thermal diffusion, energy losses due to ionization and the work done on the electrons by the electric field. The ions and neutrals are assumed to be in thermal equilibrium inside the cathode and a single equation is employed for the conservation of energy of the heavy species. The orifice plate temperature is set equal to the peak emitter temperature. The keeper plate temperature is set at 500 ^{o}C, and although it may deviate from this value depending on the operating condition the results presented herein are not found to be critically sensitive to this boundary condition. Sheath boundary conditions are applied at the cathode wall boundaries that include thermionic electron emission from the emitter. The model requires that the temperature of the emitter be specified. The specification of the emitter temperature requires two inputs: the peak emitter temperature $T_{w,max}$ and a non-dimensional polynomial that expresses the variation of the temperature as a function of position along the emitter. The functional form of the fit implemented in the present simulations is based on a measured[6] temperature profile for ¼–in cathode with a 40-mil orifice diameter, and is shown in Fig. 1.

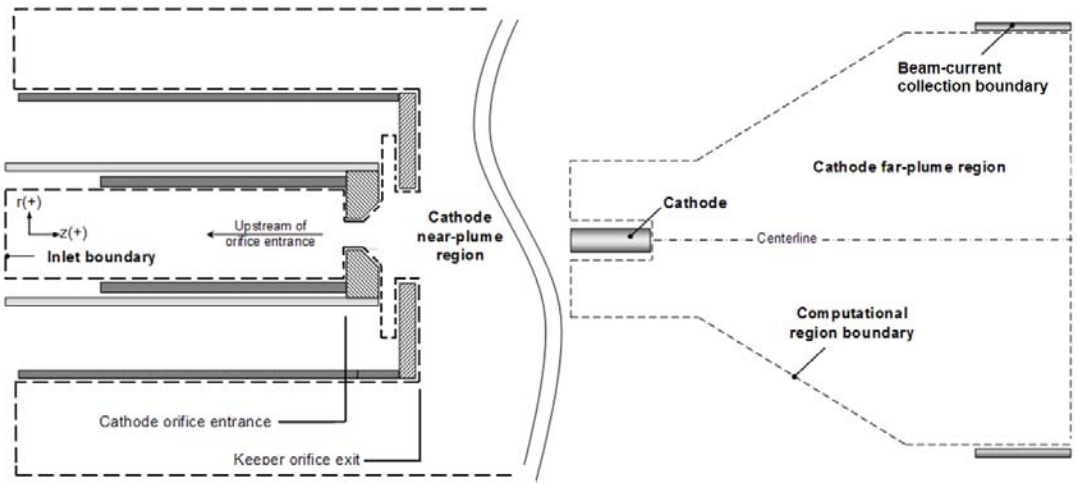

Fig. 2 The computational region employed in the NHC simulations is enclosed by the dashed line.

The neutral gas density is determined by the neutral gas continuity equation and includes the ionization source term for Xe^{+}. Inside the cathode the neutral gas viscous momentum equations are solved whereas downstream of the cathode orifice a collisionless method is employed to obtain the neutral gas density. The "fluid" and "collisionless" regions are coupled at the transition line, which in the NHC simulations is located at the exit of the cathode orifice's cylindrical section. The numerical approach for the neutral gas fluid momentum equation uses an upwind finite volume scheme by applying first-order upwind fluxes across each edge with no flux-limiting.

The computational region employed for the NHC simulations is illustrated in Fig. 2. It spans the cathode interior, cathode and keeper orifices, and the cathode's near-plume and far-plume regions. Because the size of the region is limited by the available computational resources an "electrode" boundary is placed far from the cathode to collect the beam current. The computational mesh consists mostly of

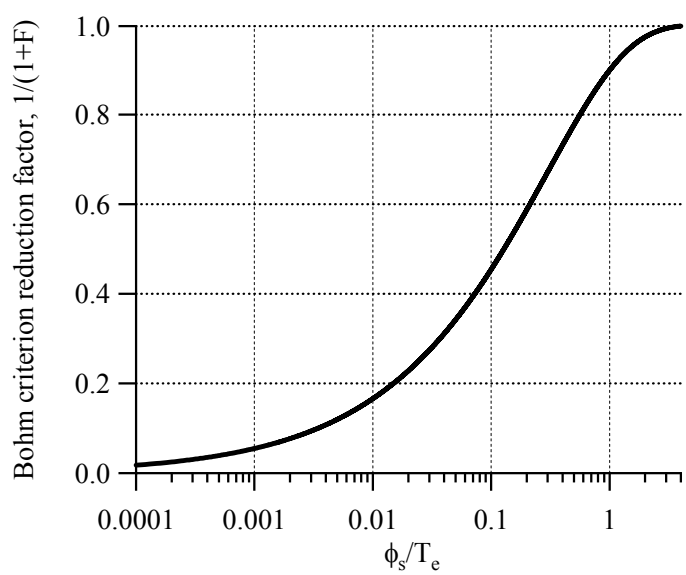

Fig. 3 The Bohm criterion reduction factor for the range of the sheath drop $0 \lesssim \phi_s/T_e < 10$. For the keeper boundary conditions related to the present work $\phi_s = \phi_p - V_K$.

rectangular cells upstream of the cathode orifice but transitions to a generalized grid arrangement in the plume region. No applied magnetic field is employed in the NHC simulations.

2) Model extensions

The existing algorithm for the boundary conditions at the keeper electrode allowed for current collection with self-consistent determination of the keeper voltage. The keeper current integrated over surface $\mathbf{S}_K$, and the sheath boundary conditions for the electron and ion current densities were previously specified in OrCa2D according to Eq. (1). Here ϕ_p-V_K is the potential drop ϕ_s across the sheath and the electron thermal flux is $j_{e,th}=n_e(8k_BT_e/\pi m_e)^{1/2}/4$. The plasma potential at the grid cell center located adjacent to the wall boundary is denoted by ϕ_p. An iterative procedure allows for the determination of V_K based on a prescribed value of the keeper current. In all simulations performed until now it had been assumed that when $\phi_p \le V_K$ the sheath is (fully) ion-repelling and no ion flux to the wall was allowed.

$$I_K = \oint\!\!\oint_{S_K} (\mathbf{j}_e + \mathbf{j}_i)\cdot d\mathbf{S}_K$$

$$\mathbf{j}_e \cdot \hat{\mathbf{n}} = \begin{cases} -j_{e,th}\, e^{-q_e(\phi_p - V_K)/k_B T_e}, & \phi_p > V_K \\ -j_{e,th}, & \phi_p \le V_K \end{cases} \qquad \mathbf{j}_i \cdot \hat{\mathbf{n}} = \begin{cases} e^{-1/2} q_e n_e \sqrt{k_B T_e / m_i}, & \phi_p > V_K \\ 0, & \phi_p \le V_K \end{cases} \tag{1}$$

In the keeper/cathode gap we find that the plasma potential spans the range between the ion-attracting and ion-repelling limits. In this intermediate regime the collected ion flux transitions smoothly from one limit (Bohm) to the other (zero flux). The implication is that if this transition is not accounted for correctly the plasma density inside the gap will be underestimated since the flux lost to the keeper is always the maximum value so long $\phi_p > V_K$, and consequently the contribution to the keeper current by $j_{e,th}$ may also be underestimated. In the present simulations the model boundary conditions have been modified in Eq. (1) as described below to account for this transition.

The speed $(k_BT_e/m_i)^{1/2}$ is a direct consequence of the so-called Bohm criterion, which requires that the plasma ions acquire translational energy from weak electric fields in the "pre-sheath." Harrison and Thompson[7] derived a general form of the criterion at the sheath edge (compared to Bohm who assumed that ions entering the sheath are mono-energetic[8]):

$$\tfrac{1}{2} m_i \left\langle u_i^{-2} \right\rangle^{-1} \ge \tfrac{1}{2} k_B T_e \tag{2}$$

where $\langle u_i \rangle$ is the mean ion velocity normal to the electrode boundary. Inherent in the analysis that leads to the criterion above is the assumption that electrons inside the sheath are characterized by the Boltzmann distribution $n_e=n_{e,\infty}\exp(-\phi_s/T_e)$ with $n_{e,\infty}$ denoting the equilibrium electron density far from the sheath. Andrews and Varey[9] showed that this is a good assumption only when the electrode is biased to a voltage that is much lower than the plasma potential. In this case the flux of electrons absorbed by the electrode is much smaller than the random flux of electrons at the sheath edge. However, as the electrode voltage is raised it is reasonable to expect that a continuous transition from the Bohm condition for the ion velocity to zero velocity as the sheath transitions from ion-attracting to ion-repelling. By taking into account the effects of the absorbed electrons Andrews and Varey derived the "Bohm reduction factor" for the case of the electrode voltage being between the floating potential and the plasma potential:

$$\tfrac{1}{2} m_i \left\langle u_i^{-2} \right\rangle^{-1} \ge \frac{\tfrac{1}{2} k_B T_e}{1 + F(\bar{\phi}_s)} \tag{3}$$

where the function $F(\bar{\phi}_s)$ is given by

$$F(\bar{\phi}_s) = \frac{e^{-\bar{\phi}_s}}{\sqrt{\pi \bar{\phi}_s}\,(1 + \mathrm{erf}\sqrt{\bar{\phi}_s})}. \tag{4}$$

with $\bar{\phi}_s \equiv \phi_s / T_e$ (and T_e expressed in eV). The last term in the denominator is the error function. The Bohm criterion reduction factor $[1+F(\bar{\phi}_s)]^{-1}$ is plotted in Fig. 3.

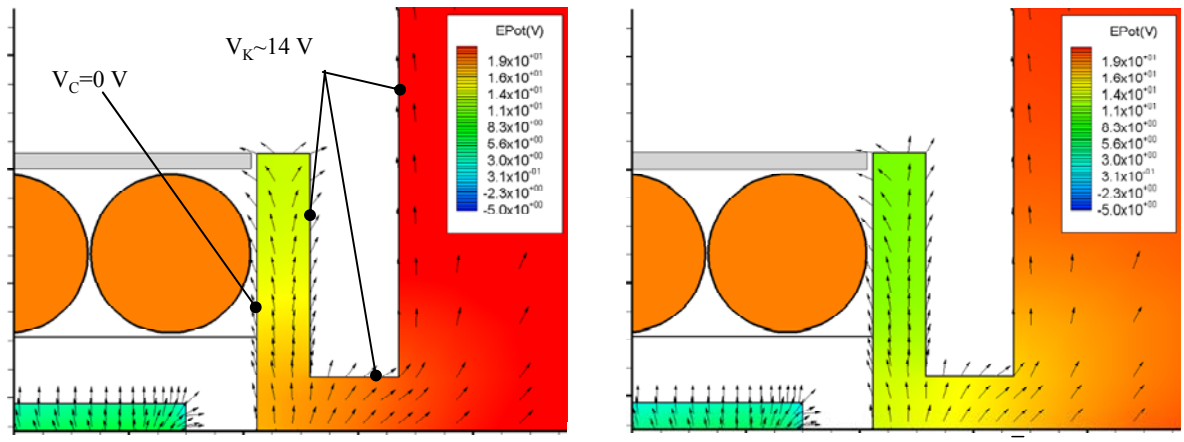

Fig. 4 Effect of the Bohm reduction factor $1/1+F(\bar{\phi}_s)$ incorporated in the keeper boundary conditions. The plots overlay plasma potential contours with the ion flux (unit) vector field. Left: Without implementation of the new model. Right: With implementation of the new model along the keeper electrode boundary.

The numerical simulation plots in Fig. 4 compare results for a typical NHC case without (left) and with (right) the new boundary condition for the ion velocity, showing clearly the reduction of the ion flux to the surface of the keeper facing the cathode; this is where the plasma potential is comparable to the keeper voltage. The effect is reduced along surfaces where the plasma potential is higher than the keeper voltage by several volts or more. We found that the effect of the improved boundary condition is to change the keeper voltage by as much as a few volts.

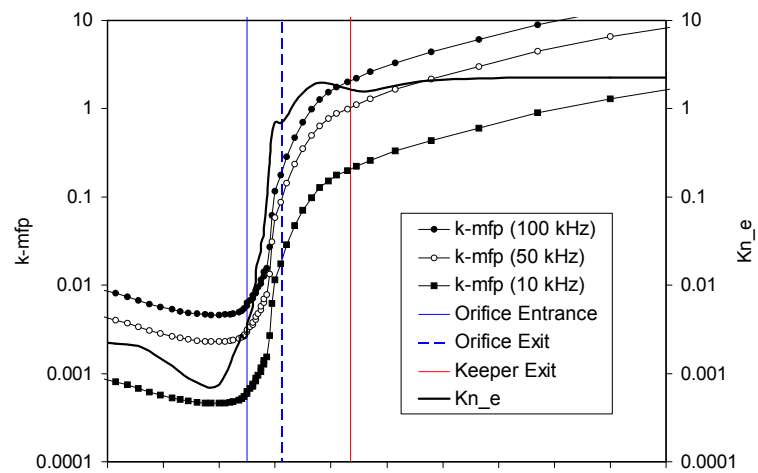

Fig. 5 The computed product $k\lambda_{mfp} \approx 2\pi f \lambda_{mfp}/C_s$ (left axis) and the electron Knudsen number, Kn_e (right axis) as a function of position along the axis of symmetry in a typical NHC. (The vertical lines show relevant locations of the orifice and keeper).

A second upgrade of the OrCa2D physics algorithms is related to the collision frequency of the electrons due to wave motion. It has recently been postulated that low-frequency (~100 kHz) turbulence, which has been predicted[10] and measured[11] in the near plume of electric propulsion cathodes, can enhance the collision frequency of the electrons in this region but a functional form of the effective resistivity has been elusive. The difficulty has been largely due to the fact that the saturation of electron-ion streaming instabilities to low-frequency turbulence in these devices is strongly dependent on both the electron drift speed (relative to the ions), which tends to drive the instability, and on collisions with ions,[12,13] neutrals and walls, which tend to damp it. Existing theories that provide approximate expressions for the collision frequency are based usually on restrictive assumptions such as collisionless and homogeneous plasma none of which applies to the pertinent regions of the cathode plasma. Previous attempts for a phenomenological model of the collision frequency in cathodes assumed a functional dependence on the electron Mach number, which we have found here in the present simulations to lead to exceedingly high electron heating under certain operating conditions and orifice geometries.

To assess the damping of wave motion in the electron flow we plot in Fig. 5 the variation of $k\lambda_{mfp}$ along the cathode centerline, approximated as shown in Eq. (5) using the ion-acoustic speed $C_s=(k_B T_e/m_i)^{1/2}$. Here the collision mean-free-path (mfp) accounts for both the electron-ion and electron-neutral interactions $\lambda_{mfp} \sim u_{T,e}/(\nu_{ei}+\nu_{en})$.

$$k\lambda_{mfp} \approx \frac{2\pi f}{C_s}\lambda_{mfp} \tag{5}$$

Because the wave frequency is unknown, we plot in Fig. 5 $k\lambda_{mfp}$ for three representative values, f=100, 50 and 10 kHz. For all cases the largest variation of $k\lambda_{mfp}$ (a few orders of magnitude) is observed in the region between the entrance to the cathode orifice and the exit of the keeper electrode where its value approaches or exceeds unity. The latter implies a higher probability for excitement of ion-acoustic turbulence in this region whereas the much smaller values near the orifice entrance suggest strong damping or no wave growth at all since the collision mfp there is much smaller than the ion-acoustic wavelength. The similarity of the variation of the electron Knudsen number, defined below as

$$Kn_e \equiv \frac{|\nabla n_e|}{n_e} \frac{u_{T,e}}{\nu_{ei} + \nu_{en}}, \tag{6}$$

with $k\lambda_{mfp}$ suggests a plausible, albeit highly idealized, approach to capture the dependence of the wave growth and in turn of the effective collision frequency ν_a on particle collisions, using the phenomenological expression in Eq. (7). In the present simulations we have incorporated Eq. (7) in the form of $\nu_a = aKn_e\omega_{pe}$ where "a" is a constant that depends on the orifice geometry, and a numerical value that we specify based on the guidance of test simulations cases to be ~0.4. In all final simulation cases presented here this numerical value has been kept fixed (unless varied for model uncertainty assessments) to eliminate the dependence of the computed trends on this parameter.

$$\nu_a \sim Kn_e\omega_{pe} \tag{7}$$

B. Comparisons of Simulation Results with Laboratory Data

1) Cases simulated

To extend the validation of the cathode model cases of orifice geometries and operating levels have been selected that span a relatively wide range of conditions for the ionized gas in these devices. Wherever model inputs (such as the emitter temperature) are unknown, or critical models (such as the numerical value of the effective collision frequency) are uncertain, sensitivity calculations have been performed to quantify such uncertainties. The results of these sensitivity calculations are presented later along with the base-case simulation results. Table 1 below lists the different cases we have simulated. The naming convention we follow for the various cathode cases is a numerical value followed by two letters that identify the operating point as high-power (HP) or low-power (LP). Finally, we note that the section of the cathode orifice that is occupied by a conical piece in many EP cathodes, commonly known as the "bevel section", does not employ the conical feature in the 30-XX and 40-XX cathodes studied here. Thus, for these cases the "bevel section" is simply an extension of the orifice's cylindrical section.

Table 1. Neutralizer cathode cases simulated with OrCa2D. All geometry related values have been normalized with respect to the 20-HP cathode.

Cathode parameter	20-HP	30-LP	30-HP	40-LP
Cathode tube diameter	1	1	1	1
Emitter length	1	1	1	1
Cathode plate orifice diameter	1	3/2	3/2	2
Keeper plate orifice diameter	1	1	1	1
Keeper plate thickness	1	0.5	0.5	0.5
Cathode-keeper gap	1	1	1	1
Mass flow rate (sccm)	4.0	1.5	3.0	1.5
Discharge voltage, V_d (V)	17.3	23.2	21.0	25.9
Keeper voltage, V_K (V)	12.7	15.25	11.5	12.85
Keeper current, I_K (A)	3.0	1.0	1.0	1.0
Beam current, I_b (A)	3.5	1.5	3.0	1.5

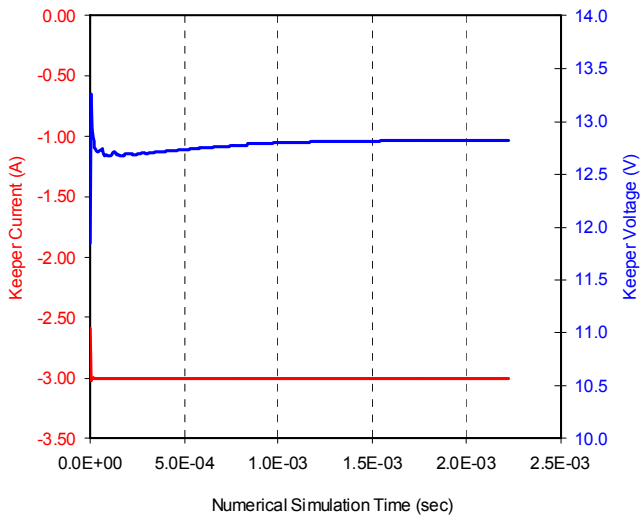

Fig. 6 Typical evolution of the computed keeper current and voltage to steady state. (Case: 20-HP).

2) Results

In this section a series of simulation results are presented, accompanied by sensitivity calculations, comparisons with plasma measurements taken along the axis of symmetry and comparisons with the observed keeper voltage. We note that dimensions in all ensuing graphical representation of the results have been intentionally omitted for propriety reasons. The numerical simulations were performed using the same computational region as shown in Fig. 2, modified for each cathode case only to account for the different orifice size. The data comparisons are performed with simulation results that show small to no variation with numerical simulation time. The keeper voltage and keeper current traces in Fig. 6 are for the 20-HP cathode and are typical for all simulations. Depending on the geometry, initial conditions and operating point the numerical simulation time to steady state ranged from a few to several milliseconds. The plasma data ranged from the keeper exit region to several centimeters downstream of the keeper, and were obtained using Langmuir probes in a laboratory vacuum chamber. The NHC was operated in an ion-engine simulated environment but without the ion engine present. The overall diagnostics system and test chamber have been described in several previous publications (e.g. see Ref. 14). The background pressure during the tests was in the low values of 10^{-5} Torr. Unless otherwise stated the simulations have assumed a value of 10^{-5} Torr.

Because the plasma density falls by several orders of magnitude in the plume region of these devices probe collection spans in all cases presented here both the thin-sheath and Orbit Motion Limited (OML) regimes. Thus, probes of different geometries have been used, and the methods to analyze the data at the two different limits have been based on well-known probe theories. A comparison between the simulation results and the density data is shown in Fig. 7. Our largest uncertainty in the plasma density comparisons lies in the intermediate regime between the thin-sheath and OML limits. Simulations to asses the sensitivity of the solution on the computational grid inside the orifice, where the steepest plasma gradients develop, show negligible changes with the resolved grid of Fig. 8, right. Thus, all results presented in this paper have used the grid arrangement shown in Fig. 8, left. The comparison of the plasma potential and electron temperature for the 20-HP cathode are shown in Fig. 9. It is found that this cathode exhibits the lowest electron temperature and that the contribution of the effective collision frequency ν_a to the total classical frequency is the smallest by comparisons to all the other cathodes. The inclusion of excitation losses in the electron energy law (in addition to the ionization losses already accounted for in all simulations) show negligible differences. All the different simulation cases and comparisons with the measured keeper voltage are listed in Table 2.

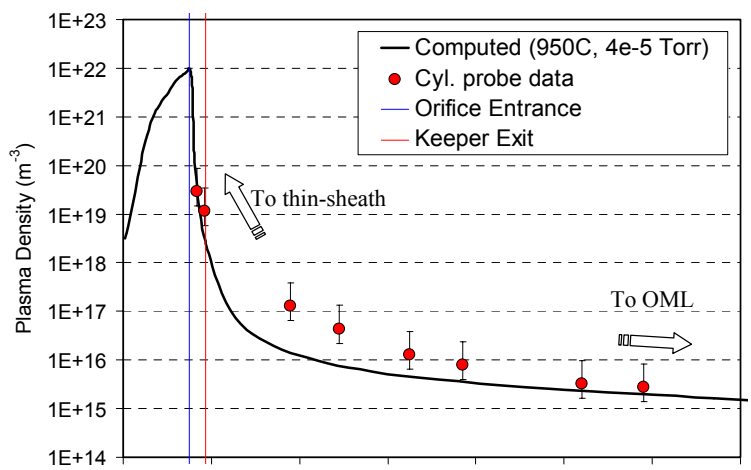

Fig. 7 Comparison of the numerical simulation result with the plasma density data along the axis of symmetry of the 20-HP cathode. The computed results assumed a peak emitter temperature $T_{w,max}$=950 C and a background pressure of 4e-5 Torr.

It has already been shown in previous work by the authors that the numerical simulation of the neutral gas in these devices is challenging because the gas transitions from collisional (Kn_n<<1) to collisionless (Kn_n>>1), and in most NHC cases this occurs inside the cathode orifice. The approach followed in OrCa2D is to model the two

regions using conventional fluid methods in the collisional regions and an approximate approach that uses view factors to compute the neutral fluxes and densities in the collisionless regions. The two regions are united at a "transition boundary" or "line" inside the orifice that is chosen arbitrarily to be at the Kn_n~1 location. The contour plots in Fig 10 show two different locations of the transition line chosen for the purpose of performing sensitivity simulations. The profiles in Fig. 11 combine the effects of different transition line locations and a=0 (i.e. no contribution from the effective collision frequency ν_a) and compare the results with the original simulation (Fig. 9) performed at a higher background pressure (4e-5 Torr) than the nominal value (1e-5 Torr), and with the data. It is found that the higher background pressure has a negligible effect on the near-plume plasma solution whereas the combined effects of collisional-to-collisionless transition and effective electron collision frequency lead to a noticeably colder electron flow, the latter of which plays the dominant role.

Table 2. Description of the various simulation cases and comparisons between the measured and computed keeper voltage (see Figs 9, and 11-15).

Simulation Cases	Keeper Voltage (V_K) Comparison		Reference
	Measured (V)	Computed (V) /Simulation case	
(1) Both ionization and excitation losses included – the "nominal simulation case" (solid line) (2) Only ionization losses accounted for in the electron flow (dashed line). The peak emitter temperature for both cases was $T_{w,max}$=950 ^oC	12.7	12.8 / (1)	Fig. 9
(1) Nominal case with a background pressure of P=4e-5 Torr (solid line) (2) Background pressure P=4e-5 Torr, no effective collision frequency ν_a (a=0), collisionless-to-collisional transition boundary located at the orifice entrance (dashed line)	12.7	13.4 / (1) 12.8 / (2)	Fig. 11
(1) $T_{w,max}$=950 ^oC (solid line) (2) $T_{w,max}$=1000 ^oC (dashed line)	11.5	12.1 / (1) 11.25 / (2)	Fig. 12
(1) $T_{w,max}$=950 ^oC (solid line) (2) $T_{w,max}$=900 ^oC (dashed line)	15.25	13.3 / (1) 14.9 / (2)	Fig. 13
(1) $T_{w,max}$=1050 ^oC (solid thick line). (2) $T_{w,max}$=1000 ^oC (solid thin line). (3) $T_{w,max}$=950 ^oC (dashed line)	12.85	11.5 / (1) 11.9 / (2) 12.4 / (3)	Fig. 14
(1) Numerical value of effective collision frequency coefficient a=0.4 (thick line) (2) Numerical value of effective collision frequency coefficient a=0.2 (thin line)	12.85	11.5 / (1) 11.4 / (2)	Fig. 15

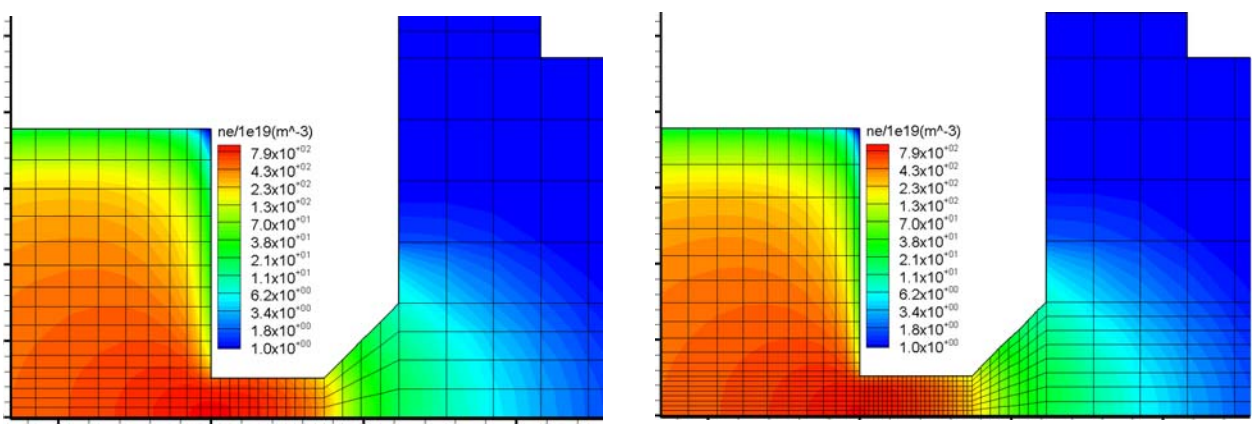

Fig. 8 Contour plots of the computed plasma density in the 20-HP cathode. The sensitivity of the numerical simulation results on the orifice grid resolution is found to be negligibly small for the coarse (left) and resolved (right) arrangements. All numerical results presented in this paper have been produced with the coarser grid (left).

The comparisons for the 30-HP, 30-LP and 40-LP cathodes are shown in Figs 12, 13 and 14, respectively. The simulation results show elevated electron temperatures by comparison to the 20-HP cathode. We find this to be due to a larger contribution of the non-classical collision frequency ν_a to the heating of the electrons. The largest discrepancy between theory and experiment is observed in the 40-HP (Fig. 14) where the LP operating condition for the given orifice size has excited strong plasma oscillations by comparison to the 30-XX, as shown in Fig. 15 (left). Thus our uncertainty on the numerical value of the constant "a" is the largest for this case. A sensitivity calculation compares the simulation result in Fig. 15 (right) for a=0.2 and a=0.4.

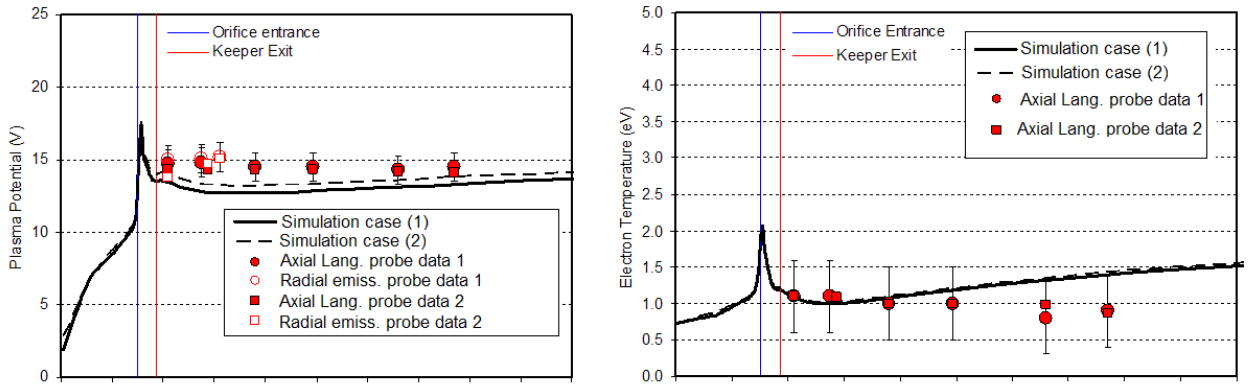

Fig. 9 Comparisons for the 20-HP cathode. The peak emitter temperature for both simulation cases was $T_{w,max}$=950°C.

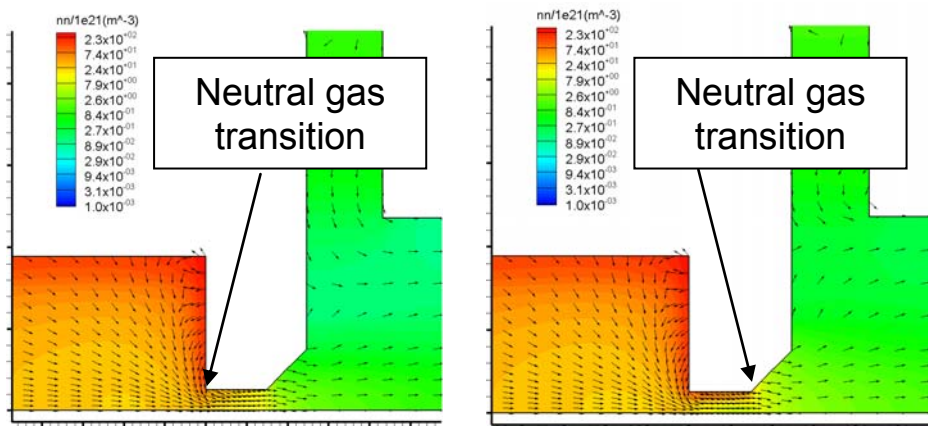

Fig 10. Contour plots of the neutral gas density in the 20-HP cathode for different choices locations of the collisionless-to-collisional transition boundary. The arrangement on the right is the nominal simulation case.

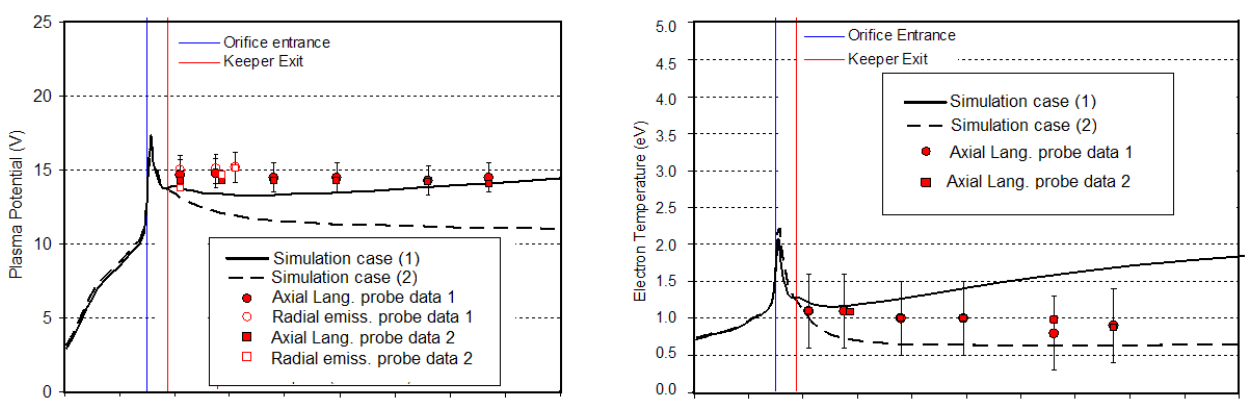

Fig. 11 Comparisons and sensitivity of simulation results on uncertain model inputs for the 20-HP cathode. For both cases $T_{w,max}$=950 °C.

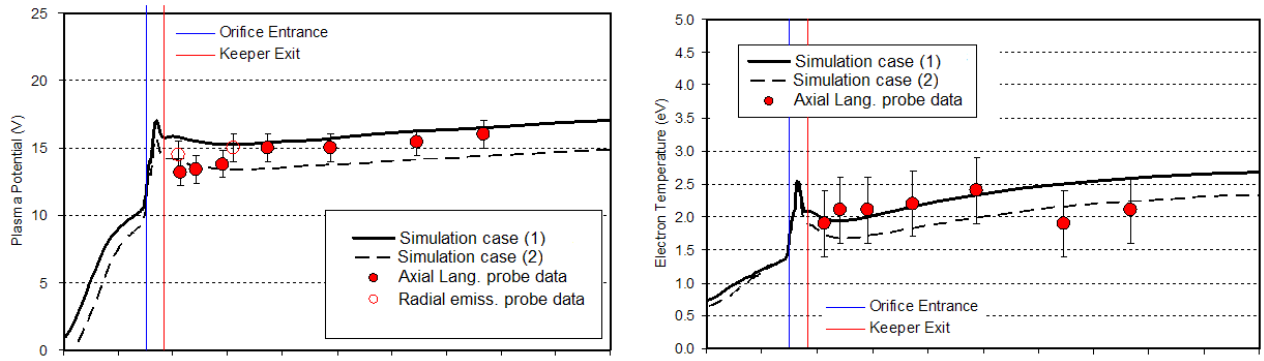

Fig. 12 Comparisons and sensitivity of simulation results on uncertain model inputs for the 30-HP cathode.

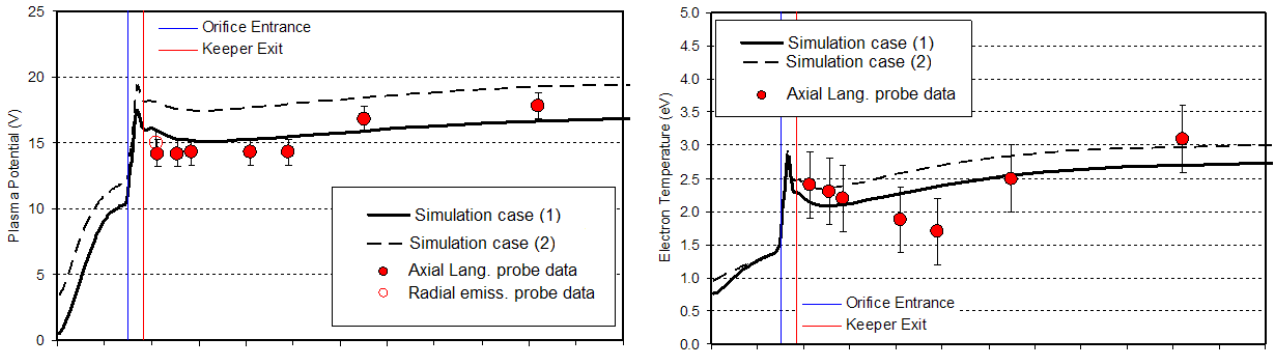

Fig. 13 Comparisons and sensitivity of simulation results on uncertain model inputs for the 30-LP cathode.

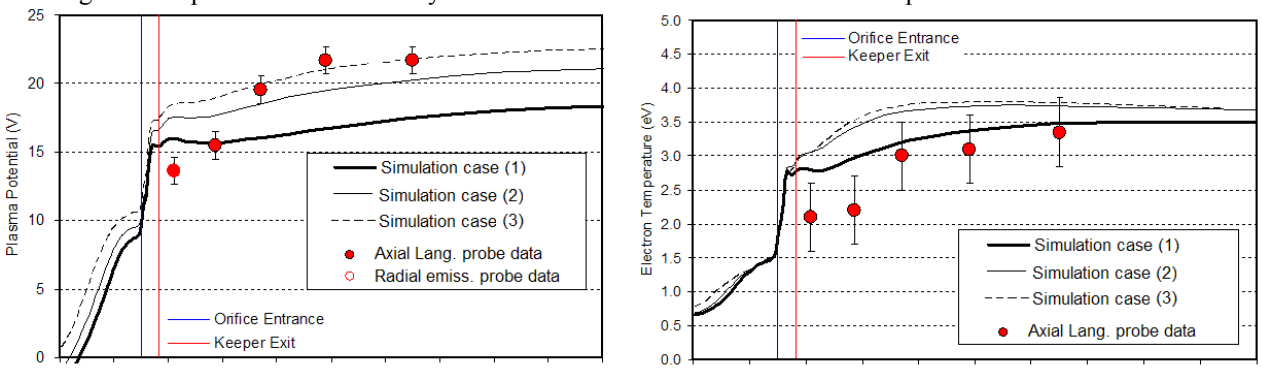

Fig. 14 Comparisons and sensitivity of simulation results on uncertain model inputs for the 40-LP cathode.

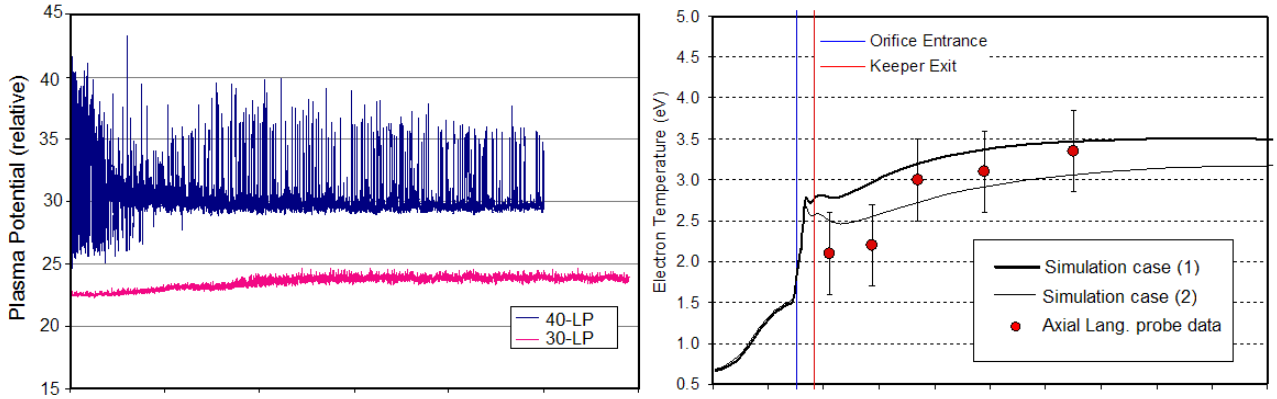

Fig. 15 Left: Plasma potential fluctuations as a function of radial position from the axis of symmetry, measured 3 mm downstream of the keeper in 30-LP and 40-LP cathodes. Right: Comparisons and sensitivity of simulation results on uncertain model inputs for the 40-LP cathode along the axis of symmetry ($T_{w,max}$=1050 ^{o}C for both cases).

III. Conclusion

This paper presented results from numerical simulations of four different neutralizer cathode cases. The simulations employed the two-dimensional computer code OrCa2D that solves numerically an extensive system of conservation laws for the partially-ionized gas in these devices. The simulation results for the plasma have been compared directly with an extensive set of laboratory measurements. The computed keeper voltage has also been compared with the value recorded during the experiments. The different cathode cases chosen for the simulations and tests were intentionally selected to span a relatively wide operation range for EP neutralizers. The goal has been to identify the validity range of the OrCa2D model as well as operation regimes of increased uncertainty. We conclude that although several areas in cathode physics remain challenging the global properties and trends observed in the cathode tests are reproduced by the numerical simulations with acceptable agreement. This establishes OrCa2D as a useful computational tool for cathode design guidance as well as for extended cathode studies in areas that remain elusive, such as such the plasma wave motion and the (likely related) mechanisms that drive these devices to plume-mode operation.

Acknowledgments

The research described in this paper was carried out by the Jet Propulsion Laboratory, California Institute of Technology, under a contract with the National Aeronautics and Space Administration. Reference herein to any specific commercial product, process, or service by trade name, trademark, manufacturer, or otherwise, does not constitute or imply its endorsement by the United States Government or the Jet Propulsion Laboratory, California Institute of Technology. Portions of the work described herein were funded by NASA's In-Space Propulsion Technology Program under the NEXT Project, led by the NASA Glenn Research Center, with Scott Benson as the Project Manager and Mike Patterson as the Principal Investigator.

References

[1] Mikellides, I. G., Katz, I., Goebel, D. M., Jameson, K. K., and Polk, J. E., "Wear Mechanisms in Electron Sources for Ion Propulsion, II: Discharge Hollow Cathode," *J. Prop. Power*, Vol. 24, No. 4, 2008, pp. 866-879.
[2] Mikellides, I. G., Katz, I., Goebel, D. M., and Polk, J. E., "Assessments of Hollow Cathode Wear in the Xenon Ion Propulsion System (XIPS©) by Numerical Analyses and Short-Duration Tests," AIAA Paper 08-5208, July 2008.
[3] Patterson, M.J., and Benson, S.W., "NEXT Ion Propulsion System Development Status and Performance," AIAA Paper 07-5199, July 2007.
[4] Herman, D.A., Soulas, G.C., and Patterson, M.J., "Performance Characteristics of the NEXT Long-Duration Test after 16,550 h and 337 kg of Xenon Processed," AIAA Paper 08-4527, July 2008.
[5] Mikellides, I. G., and Katz, I., "Wear Mechanisms in Electron Sources for Ion Propulsion, I: Neutralizer Hollow Cathode," *J. Prop. Power*, Vol. 24, No. 4, 2008, pp. 855-865.
[6] Polk, J. E., Marrese, C., Thornber, B., Dang, L., and Johnson, L., "Temperature Distributions in Hollow Cathode Emitters," AIAA Paper 04-4116, July 2004.
[7] Harrison, E. R., and Thompson., W. B., "The Low Pressure Plane Symmetric Discharge," *Proc. Phys. Soc.* 74, No. 2, 1959, pp. 145-152.
[8] Bohm, D., 1949, *The Characteristics of Electrical Discharges in Magnetic Fields*, Eds A. Guthrie and R. K. Wakerling (New York: McGraw-Hill), chap. 3.
[9] Andrews, J. G., And Varey, R. H., "The Sheath at an Electrode Close to Plasma Potential," *J. Phys. A: Gen. Phys.*, 1970, Vol. 3, pp. 413-420.
[10] Mikellides, I. G., Katz, I., Goebel, D. M., and Polk, J. E., "Hollow Cathode Theory and Experiment, II. A Two-Dimensional Theoretical Model of the Emitter Region," *J. Appl. Phys.*, Vol. 98, No. 11, 2005, pp. 113303 (1-14).
[11] Goebel, D. M., Jameson, K. K., Katz, I., and Mikellides, I. G., IEPC Paper 2005-269, October 2005.
[12] Epperlein, E. M., Short, R. W., and Simon, A. "Damping of Ion-Acoustic Waves in the Presence of Electron-Ion Collisions," *Phys. Rev. Letters*, Vol. 69, No. 12, 1992, pp. 1765-1768.
[13] Maksimov, A. V., and Silin, V. P., "Damping of Ion Acoustic Waves in a Plasma with Rare Collisions in Connection with Nonlocal Hydrodynamics," *JETP Lett.*, Vol. 59, No. 8, 1994, pp. 534-536.
[14] Goebel, D. M., Jameson, K. K., Watkins, R. M., Katz, I., and Mikellides, I. G., "Hollow Cathode Theory and Experiment, I. Plasma Characterization Using Fast Miniature Scanning Probes," *J. Appl. Phys.*, Vol. 98, No. 11, 2005, pp. 113302 (1-9).